

Nanowire Aptasensors for Electrochemical Detection of Cell-Secreted Cytokines

Ying Liu,^{†,‡,§,¶,||} Ali Rahimian,^{†,¶,||,§} Sergiy Krylyuk,^{§,||} Tam Vu,[†] Bruno Crulhas,[†] Gulnaz Stybayeva,^{‡,¶} Meruyert Imanbekova,^{†,‡} Dong-Sik Shin,^{†,●} Albert Davydov,^{§,||} and Alexander Revzin^{*,†,¶,||}

[†]Department of Biomedical Engineering, University of California, Davis, Davis, California 95616, United States

[‡]State Key Laboratory of Analytical Chemistry for Life Science, School of Chemistry & Chemical Engineering, Nanjing University, Nanjing, 210008, China

[§]Materials Science and Engineering Division, Materials Measurement Laboratory, National Institute of Standards and Technology, Gaithersburg, Maryland 20899, United States

^{||}Institute for Research in Electronics and Applied Physics, University of Maryland, College Park, Maryland 20742, United States

[‡]National Center for Biotechnology of the Republic of Kazakhstan, 010000 Astana, Kazakhstan

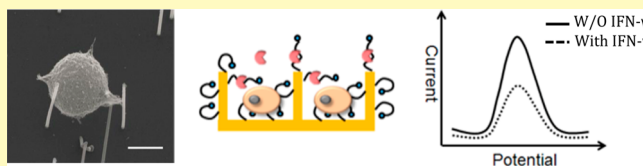
[¶]Department of Physiology and Biomedical Engineering, Mayo Clinic, Rochester, Minnesota 55905, United States

[●]Department of Chemical Engineering, Sookmyung Women's University, Seoul 140-742, Republic of Korea

ABSTRACT: Cytokines are small proteins secreted by immune cells in response to pathogens/infections; therefore, these proteins can be used in diagnosing infectious diseases. For example, release of a cytokine interferon (IFN)- γ from T-cells is used for blood-based diagnosis of tuberculosis (TB). Our lab has previously developed an aptamer-based electrochemical biosensor for rapid and sensitive detection of IFN- γ .

In this study, we explored the use of silicon nanowires (NWs) as a way to create nanostructured electrodes with enhanced sensitivity for IFN- γ . Si NWs were covered with gold and were further functionalized with thiolated aptamers specific for IFN- γ . Aptamer molecules were designed to form a hairpin and in addition to terminal thiol groups contained redox reporter molecules methylene blue. Binding of analyte to aptamer-modified NWs (termed here nanowire aptasensors) inhibited electron transfer from redox reporters to the electrode and caused electrochemical redox signal to decrease. In a series of experiments we demonstrate that NW aptasensors responded 3 \times faster and were 2 \times more sensitive to IFN- γ compared to standard flat electrodes. Most significantly, NW aptasensors allowed detection of IFN- γ from as few as 150 T-cells/mL while ELISA did not pick up signal from the same number of cells. One of the challenges faced by ELISA-based TB diagnostics is poor performance in patients whose T-cell numbers are low, typically HIV patients. Therefore, NW aptasensors developed here may be used in the future for more sensitive monitoring of IFN- γ responses in patients coinfecting with HIV/TB.

KEYWORDS: electrochemical biosensor, IFN- γ aptamer, nanowire electrode, aptasensor, tuberculosis detection



Nanostructures such as nanowires (NWs) offer interesting advantages for sensing related to geometry, electrical conductivity, and high surface area-to-volume ratio. Recent studies have shown the wide application of NWs as biosensor devices,^{1,2} cell culture substrates,^{3,4} and drug delivery vehicles.⁵ NW-based devices have also been used for stimulating, recording from, and delivering objects to single cells and tissues.⁶

Vertically grown NWs have become increasingly popular recently for cell culture and analysis. Recent studies demonstrated vertical NWs for penetrating the cell membrane and delivering a variety of biomolecules including siRNA, peptides, DNA, and proteins into primary neurons and fibroblasts.^{7,8} "Nanostraw" structures have also been applied to build a fluidic connection for direct cytosolic access and molecule delivery.⁹

In addition to intracellular delivery, vertical NWs have been used for intracellular and extracellular biosensing. Nano-

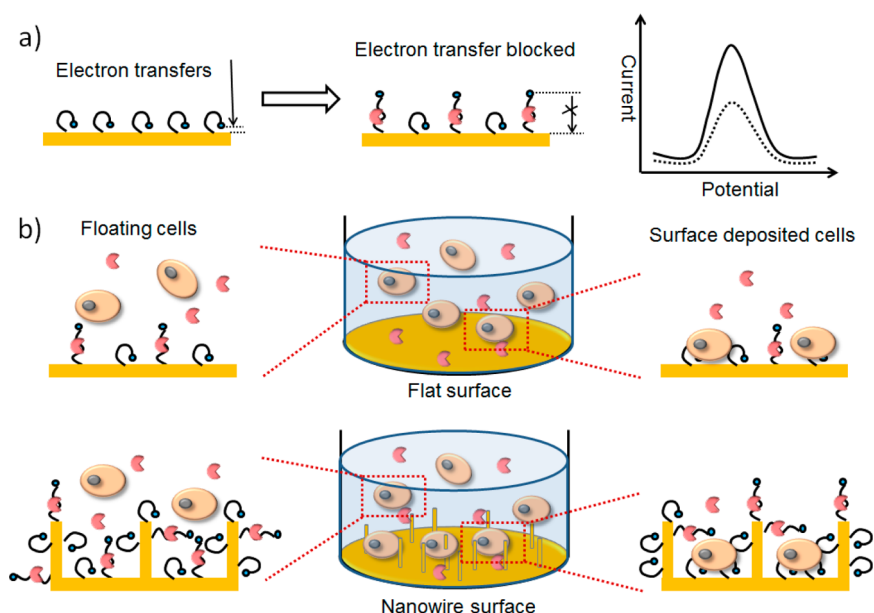
structured surfaces are particularly attractive in electrochemistry where such surfaces enhance diffusion, decrease response times, and improve electrode sensitivity.¹⁰ Lieber's group developed arrays of nanofield effect transistors (nanoFET) based on vertical NWs and demonstrated intracellular recording of transmembrane potential from a single cardiomyocyte.^{11,12} Kelley's group has developed nanostructured electrodes that allowed detection of bacterial nucleic acids at attomolar concentration.^{13,14} The same group integrated nanostructured microelectrodes with microfluidic lysis of cancer cells for detection of intracellular RNA.¹⁵

Our lab has been interested in developing biosensors for monitoring cell function,^{16–18} with particular emphasis placed

Received: July 14, 2017

Accepted: September 26, 2017

Scheme 1. (a) Schematic of the Aptamer-Based Electrochemical Sensor for IFN- γ ⁴; (b) Different Behaviors of Cell Deposition and Cytokine IFN- γ Secretion for Floating Cells and Surface Deposited Cells on Planar Au Electrode and AuNWs Electrode



⁴The aptamer was originally in a hairpin structure and the redox label was in close proximity to the electrode surface. Upon IFN- γ binding, the hairpin changed conformation and the redox label moved further away from the electrode, lowering the electron-transfer efficiency. The differences in the faradaic current before and after IFN- γ binding were quantified using square wave voltammetry (SWV).

on methods that allow continuous monitoring of cellular secretions.^{19–21} We have previously reported on the development of electrochemical aptasensors for detection of IFN- γ and other cytokines.^{22,23} These aptasensors function as proposed by Plaxco group and others^{24–26} and described in Scheme 1. Binding of analyte to aptamer-functionalized electrode causes a change in aptamer structure, decreases (or increases) rate of electron transfer, and shifts the electrochemical redox signal. We hypothesized that advantages of nanostructured surfaces—improved transport and enhanced surface area per footprint—would result in more sensitive aptasensors for analysis of cell-secreted signals. Therefore, we employed Au-covered vertical Si NWs as working electrodes for aptamer-based detection of IFN- γ , an important inflammatory cytokine. Nanostructured electrodes had 3.18-fold faster response time and 3.90-fold better sensitivity to IFN- γ compared to standard flat electrodes. Most strikingly, nanostructured aptasensors enabled detection of IFN- γ release from as few as 150 T-cells per mL of solution. Standard IFN- γ ELISA was not sensitive enough to detect a signal from such a low number of cells.

EXPERIMENTAL SECTION

Materials. HEPES, sodium chloride (NaCl), potassium chloride (KCl), magnesium chloride (MgCl₂), sodium bicarbonate (NaHCO₃), dimethylformamide (DMF), 6-mercapto-1-hexanol (MCH), tris(2-carboxyethyl) phosphine hydrochloride (TCEP), (3-aminopropyl)-trimethoxysilane (APTMS), *N,N*-diisopropylethylamine (DIPEA), bovine serum albumin (BSA), paraformaldehyde (PFA), and T cell activation reagents, phorbol 12-myristate-13-acetate (PMA) and ionomycin, were purchased from Sigma-Aldrich (St. Louis, MO). [Note: Certain commercial equipment, instruments, or materials are identified in this paper in order to specify the experimental procedure adequately. Such identification is not intended to imply recommendation or endorsement by the National Institute of Standards and Technology, nor is it intended to imply that the materials or equipment identified are necessarily the best available for the purpose.]

Silicon wafer was purchased from WRS materials (San Jose, CA) and coated with gold in LGA Thin films (Santa Clara, CA). Human recombinant Interferon gamma (IFN- γ), tumor necrosis factor alpha (TNF- α), Interleukin-12 (IL-12), Interleukin-6 (IL-6), Interleukin-10 (IL-10), and ELISA kit were purchased from R&D systems (Minneapolis, MN). FITC Mouse Anti-Human CD3 antibody was obtained from BD Pharmingen. Cell culture medium RPMI 1640 with L-glutamine, Alexa Fluor 488 carboxylic acid succinimidyl ester, Alexa Fluor 594 carboxylic acid succinimidyl ester, fluorescence-based live/dead cell viability kit were purchased from Life Technologies (Carlsbad, CA), and CellTracker Green CMFDA dye. One step NBT/BCIP Western blotting test kit was purchased from Thermo Scientific (Waltham, MA). Methylene blue-carboxylic acid succinimidyl ester (MB-NHS) was purchased from Biosearch Technologies Inc. (Novato, CA). Jurkat cell line was obtained from ATCC.

The IFN- γ -binding aptamer was synthesized by IDT Technologies (San Diego, CA). The 34-mer IFN- γ -binding aptamer sequence was as follows: 5'-NH₂-C6-GGG GTT GGT TGT GTT GGG TGT TGT GTC CAA CCC C-C3-SH-3'. IFN- γ aptamer was modified at the 3-terminus with a C3-disulfide [HO(CH₂)₃-S-S-(CH₂)₃-] linker and at the 5-terminus with an amine group for redox probe (MB) conjugation. The aptamers were dissolved in HEPES buffer (10 mM HEPES, 150 mM NaCl, 5 mM KCl, 5 mM MgCl₂) (pH 7.4). Thiolated aptamer was reacted with 10 mM TCEP for 1 h at room temperature to reduce the disulfide bond of the probe.

Conjugation of Redox Reporter to Aptamers. The redox reporter MB-NHS was conjugated to the 5'-terminus of amino modified IFN- γ aptamer through succinimide ester coupling following previously reported protocols.²² Briefly, 0.5 M NaHCO₃ was added to 100 μ M aptamer solution to adjust solution pH, followed by the addition of MB-NHS for conjugation. The mixture solution was stirred and allowed to react for 4 h at 4 °C in the dark. After conjugation, MB-IFN- γ was filtered using centrifugal filter (Millipore, Amicon Ultra 3K 0.5 mL) and stored at -20 °C before use.

Growth of Silicon Nanowires. Silicon nanowires (Si NWs) were grown in a hot-walled chemical vapor deposition (CVD) system as reported elsewhere.²⁷ Briefly, gold nanoparticles (Au NPs), which served as the nucleation centers for Si NWs according to the vapor-liquid-solid (VLS) mechanism, were randomly dispersed on poly(L-

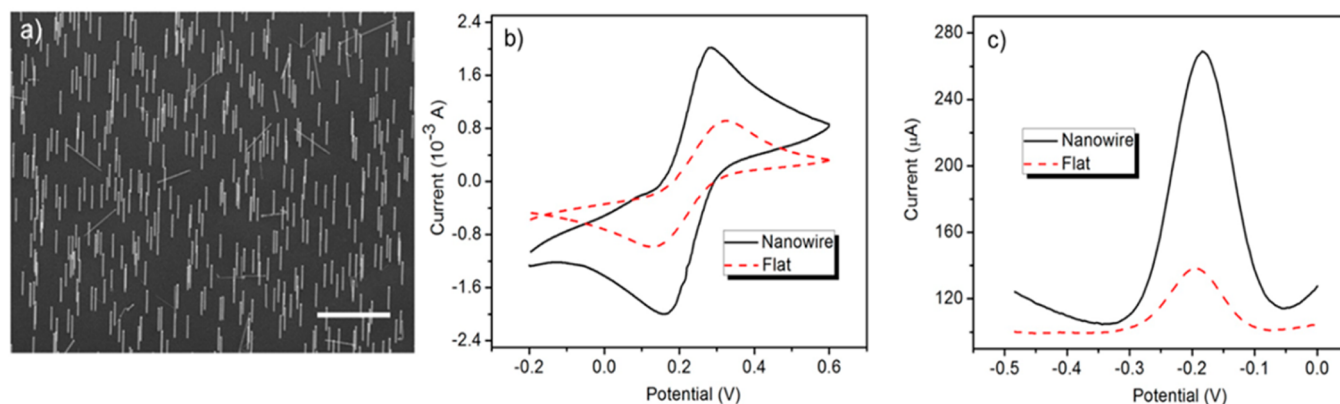


Figure 1. Characterization of NW electrodes: (a) SEM of vertical nanowires at 30° tilt view. Scale bar—10 μm . (b) Cyclic voltammetry of planar Au (red dash line) and NW electrode (black solid line) in 5 mM $[\text{Fe}(\text{CN})_6]^{3-}$ containing 0.1 M KCl at scanning rate of 100 mV s^{-1} . (c) Square wave voltammetry (SWV) for planar (red dashed line) and NW electrodes (black solid line) functionalized with IFN- γ MB aptamer.

lysine) functionalized n-Si (111) substrates by casting a droplet of Au NPs colloidal solution (Ted Pella, Inc.) followed by N_2 blow dry. Si NWs were then grown at 900 $^\circ\text{C}$ and 80 kPa reactor pressure using 10 standard cm^3/min (sccm) of SiCl_4 vapor and 200 sccm of H_2 that were diluted with N_2 carrier gas to a total flow rate of 1000 sccm. Growth duration was between 2 and 30 min to obtain NWs with target lengths of 6, 60, and 160 μm . We used monodispersed colloidal solutions of Au NPs with average diameters of 30, 100, and 200 nm, which yielded Si NWs with approximately the same diameters. Due to different density of Au NPs in colloidal solutions, surface density of the obtained Si NWs was estimated to be $(11 \pm 2) \times 10^8$ NWs/ cm^2 , $(24 \pm 4) \times 10^6$ NWs/ cm^2 , and $(5 \pm 1) \times 10^6$ NWs/ cm^2 for 30, 100, and 200 nm Au NPs, respectively. For electrochemical characterization and biosensor applications, the NW surfaces of Si substrates were sputter-coated with 10 nm Cr/30 nm Au bilayers and 10 nm Cr/100 nm Au was e-beam deposited on the backsides of the substrates.

Assembly of Electrochemical Cell and Preparation of Aptasensors. The IFN- γ aptasensor was prepared in a homemade Teflon-based sample holder/electrochemical cell. Gold coated Si NW (AuNW) substrates were placed into the sample holder, creating a cylindrical electrochemical (e)-cell with inner diameter of 10.8 mm and volume of 0.5 mL. Ag/AgCl (3 M KCl) reference electrode and a Pt wire counter electrode were immersed into e-cell for making electrochemical measurements. HEPES buffer or RPMI 1640 cell culture media were used as electrolyte.

The Au NWs or planar Si substrates Au-coated similarly to SiNW samples were cleaned with oxygen plasma, then thoroughly rinsed with DI water, and dried under nitrogen. Prior to modification of the electrodes, aptamer stock solution (50 μM) was reduced in 10 mM TCEP for 1 h to cleave disulfide bonds. This solution was then diluted in HEPES buffer to 1 μM and pipetted into the e-cell preloaded with Au NW or planar Au substrates. Aptamer solution was incubated with electrode surfaces overnight in the dark at 4 $^\circ\text{C}$. Subsequently, electrodes were rinsed with copious amounts of DI water and then immersed in an aqueous solution of 3 mM MCH for 1 h to passivate the electrode surface. As a final step, the electrodes were rinsed with DI water, dried with nitrogen, and stored at 4 $^\circ\text{C}$ prior to use.

Electrochemical Characterization of NW Electrodes and Calibration of IFN- γ Aptasensor. Electrochemical measurements were carried out with a CHI 842B potentiostat (CH Instruments, Austin, TX) operating with a three electrode system as described above. Electrochemical characterization of NW electrodes was performed using cyclic voltammetry (CV) in 5 mM $[\text{Fe}(\text{SCN})_6]^{3-/4-}$ within 0.1 M KCl. Electrochemical detection of IFN- γ from NW electrodes was performed using square wave voltammetry (SWV) with a voltage range of -0.5 to 0 V and 40 mV amplitude, 60 Hz frequency.

After assembling MB-IFN- γ aptamer, 1 mL of HEPES buffer or RPMI 1640 medium was infused into an e-cell and an electrode was allowed to equilibrate for 30 min, as determined by stable faradaic current. Small amounts of concentrated human recombinant IFN- γ

solutions were pipetted into the reaction well to adjust concentrations from 0.2 to 280 ng/mL. Before conducting SWV measurements, the sensor was allowed to react with analyte for 30 min to ensure cytokine-aptamer binding. Binding of IFN- γ caused the redox peak to shift down. The change in redox activity was reported as signal suppression—a ratio of (initial peak redox current – final peak redox current)/initial peak redox current. To demonstrate specificity, aptamer-modified electrodes were challenged with 100 ng/mL IFN- γ , as well as nonspecific cytokines including IL-12, IL-6, IL-10, and BSA.

Purification of CD4 T-Cells from Human Blood. The whole blood was collected from healthy adult donors through venipuncture under sterile conditions with informed consent and approval of the Institutional Review Board of the University of California at Davis (Protocol No. 222894–6). Peripheral blood mononuclear cells (PBMCs) were purified using a density gradient media, Lymphoprep (Axis-shield, Oslo, Norway). CD4+ T-cells were isolated from the purified PBMC population through negative selection by magnetic beads using the EasySep human CD4+ T cell enrichment kit (Stemcell Technologies, Vancouver, BC, Canada) according to the manufacturer instructions and cultured in RPMI 1640 with 10% fetal bovine serum and 1% penicillin/streptomycin (Gibco, Chino, CA, United States). The cell count and viability test was performed using 0.4% trypan blue solution on hemocytometer (Thermo Fisher scientific Inc., San Diego, CA, United States). Phorbol myristate acetate (50 ng/mL) and Ionomycin (1 $\mu\text{g}/\text{mL}$) were the stimuli used to induce secretion of IFN- γ and TNF- α (Sigma-Aldrich, St. Louis, MO, United States).

For experiments utilizing chimeric antibodies, T-cell population was isolated from the purified PBMC through negative selection by magnetic beads using the EasySep human T cell enrichment kit (Stemcell Technologies, Vancouver, BC, Canada) according to manufacturer's instructions. Isolated T cells were labeled with the IFN- γ capture chimeric antibody (Miltenyi Biotec, Bergisch Gladbach, Germany) according to the instructions provided by the manufacture and stimulated with PMA (50 ng/mL) and ionomycin (1 $\mu\text{g}/\text{mL}$). The supernatant then collected and analyzed by IFN- γ /TNF- α DuoSet ELISA kit (R&D systems, Minneapolis, MN, United States).

Scanning Electron Microscopy. 300,000 T-cells were suspended in 1 mL RPMI and cultured on 1 cm \times 1 cm NW electrode substrate for 4 h in an incubator at 37 $^\circ\text{C}$ to allow cells to settle down. The surface was then rinsed with water three times to get rid of the unattached cells and incubated in 1% aqueous solution of PFA for 15 min to fix the cells attaching to the substrate. The samples were then dehydrated in gradually increasing concentrations of ethanol (30–100%) in water, dried in a critical point dryer, and sputter-coated with a few nanometers of gold to increase conductivity for SEM characterization. As a control experiment, the same concentration of T-cells was incubated and fixed on a flat substrate.

Analysis of IFN- γ Release from T-Cells. For cell secretion experiment, the Teflon device with integrated electrodes was placed

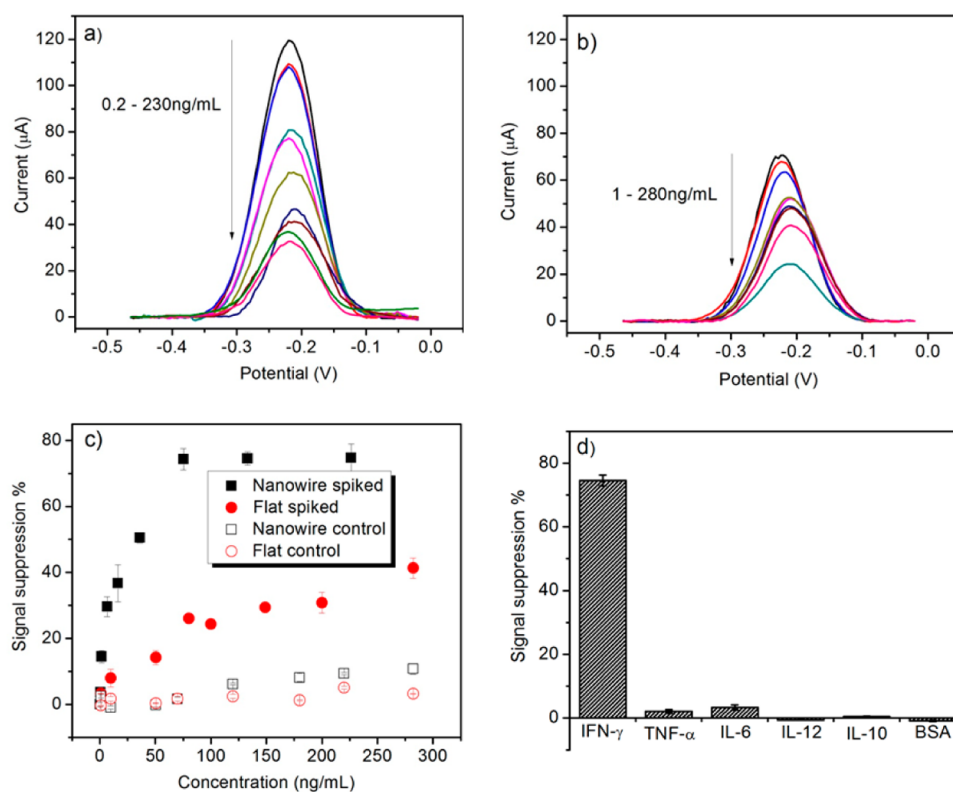


Figure 2. Performance of NW aptasensors: (a) SWV responses of NW aptasensors challenged with IFN- γ ranging from 0.2 to 230 ng/mL. (b) SWV analysis of planar aptasensors exposed to IFN- γ ranging from 1 to 280 ng/mL. (c) Calibration curves constructed by plotting sensor responses to various concentrations of cytokines for NW aptasensor (w/IFN- γ : solid black square; w/o IFN- γ : open black square) and planar aptasensor (w/IFN- γ : solid red circle; w/o IFN- γ : open red circle). The data points and error bars represent average and standard deviations of measurements from three different aptasensors. (d) Specificity of NW aptasensor. Electrodes were challenged with IFN- γ , TNF- α , IL-6, IL-12, IL-10, and BSA at 100 ng/mL. Error bars are standard deviation from the average of three different aptasensors.

into a custom-made heating incubator to maintain 37 °C and 5% CO₂. T-cell suspension in RPMI 1640 was added into an E-cell and incubated for 30 min allowing cells to settle down. Subsequently, mitogens (PMA (50 ng/mL) and ionomycin (2 mM)) dissolved in RPMI 1640 were added into e-cell to stimulate T-cells to produce cytokines. SWV measurements commenced immediately upon mitogenic stimulation and were made every 10 min for the first 50 min, every 20 min after for the course of 100 min. Different cell number from 150 to 50,000 were suspended in 1 mL RPMI 1640 media and allowed to sediment onto planar and NW electrodes. Different geometries of NW electrodes were evaluated to determine the configuration yielding the most sensitive detection.

Cell Viability Analysis. This experiment was carried out to determine whether cell viability was affected by placement into E-cell and subsequent electrochemical measurements. 300,000 T-cells were placed into an E-cell containing 0.5 mL of RPMI1640. The cells were mitogenically stimulated and IFN- γ release measurements were made over the course of 2 h. Subsequently, media was removed and cells were assessed for viability by LIVE/DEAD staining and fluorescence microscopy (Axiovert 200M, Zeiss, Germany).

RESULTS AND DISCUSSION

Characterization of NW Electrodes. Building nanostructured electrodes significantly increases electrode area per foot print, enhances analyte capture efficiency and improves analyte transport to the electrode. Figure 1a shows a typical SEM image of 100-nm-diameter NWs used in this study. As seen from this image, the majority of NWs remained upright—the orientation most optimal for function of the aptasensor. While NWs of different geometries were tested during this study, nanostructures most commonly used were 6 μ m long

and 100 nm diameter with surface grafting density of about $(24 \pm 4) \times 10^6$ NWs/cm². The NWs were randomly distributed on the surface with distances between individual nanostructures ranging from 2 to 10 μ m, which provided enough space for cells to land.

Upon sputtering Au and creating NW electrodes, we examined electrochemical properties of these electrodes using [Fe(CN)₆]^{3-/4-} cyclic voltammetry. The electrodes used in these experiments had NWs of 6 μ m height and 100 nm diameter. Figure 1b shows typical [Fe(CN)₆]^{3-/4-} cyclic voltammetry curves generated from flat and nanostructured electrodes. As seen from these data the redox peaks for nanostructured surfaces were ~ 2.5 times higher than standard flat electrodes. The enhancement in redox signaling is in good agreement with 2.3-fold enhancement in surface area of Au NW electrodes. This experiment highlights the fact that nanostructured electrode surface was easily accessible to molecules diffusing from solution. Next, we functionalized planar and NW electrodes with MB-labeled aptamers and carried out SWV analysis. As seen from Figure 1c the reduction peak current for NW electrodes was ~ 2.3 times higher than for planar electrodes. This is logical given the increase in surface area for NW electrodes. SWV curves were also used to determine aptamer density on flat and nanostructured surfaces. The MB-IFN- γ aptamer surface immobilization densities were estimated to be 5.97×10^{13} molecules/cm² for NWs electrode and 1.27×10^{13} molecules/cm² for planar Au electrode. The results were in general agreement with other reports employing MB-tagged hairpin aptamers.^{28–30} One should note that values above are

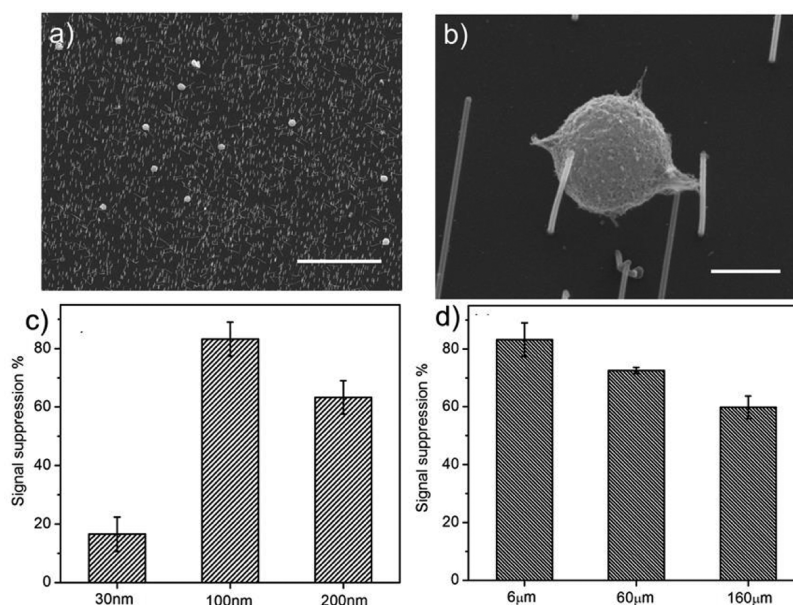


Figure 3. Effects of NW density and geometry on detection of IFN- γ from cells: (a,b) SEM images of leukocytes on electrodes with 100 nm diameter wires at 30° tilt view. Scale bar for (a) is 50 μm and for (b) is 2 μm . (c) Detection of IFN- γ from NWs of the same length (6 μm) but different diameters. (d) Detection of IFN- γ using electrodes with nanowires of the same diameter (100 nm) but different lengths.

reported for the footprint area. After accounting for higher surface area of NW electrodes, the density of aptamer molecules on the surface remains ~ 2 -fold higher compared to a planar electrode. The higher aptamer packing density on NW electrodes may be explained by curvature effects when nanostructure curvature approaches the size of a DNA molecule.³¹

Electrochemical Detection of IFN- γ Using Aptamer-Modified NW Electrodes. We have previously designed an IFN- γ beacon that contains a hairpin with stem region partially obstructing aptamer nucleotides.³⁰ As shown in Scheme 1, hairpin probes carry redox reporters (MB) so that binding of analyte molecules causes conformation of the hairpin molecules to change and redox current to decrease. The loss in signal is presented in terms of signal suppression defined as (initial redox peak current – final redox peak current)/(original redox current).

Figure 2a,b shows typical SWV voltammograms in RPMI cell culture media with MB reduction peak appearing at -0.25 V (vs Ag/AgCl). Challenging the sensing electrode with varying concentrations of recombinant IFN- γ from 0.2 to 280 ng/mL resulted in a decrease of MB redox current: the larger the concentration, the larger the decrease in redox current. The SWV results were converted into a calibration curve by plotting the normalized change in redox peak current (signal suppression) vs concentration of cytokines. The MB redox peak linearly decreased in response to the addition of IFN- γ protein for both AuNW and planar electrodes (Figure 2a,b). However, nanowire aptasensors exhibited greater changes in signal in response to IFN- γ compared to planar electrodes. The dynamic range of nanowire aptasensor reached 100 ng/mL and 75% signal suppression whereas values for planar aptasensor were 280 ng/mL and 41%. The limit of detection, calculated as $3\times$ signal/noise, was 0.14 ng/mL and 0.8 ng/mL for nanowire and planar aptasensor, respectively. Control experiments in Figure 2c refer to spiking aliquots of HEPES without IFN- γ and monitoring changes in the biosensor response. These control

experiments point to stability of the aptasensor background signal.

In addition to sensitivity and dynamic range, specificity is a key requirement for a biosensor. To demonstrate specificity, NW aptasensors were challenged with inflammatory cytokines that may be produced by immune cells, TNF- α , IL-6, IL-10, IL-12, as well as with BSA—most abundant protein in blood serum. Figure 2d demonstrated that MB redox peaks in response to different cytokines and signal suppression were all less than 5% after exposure to 100 ng/mL of nonspecific proteins. Challenging the AuNWs aptasensor with 100 ng/mL IFN- γ was used as the positive control and resulted in 75% signal suppression. This experiment highlights that nanowire aptasensors were indeed specific to the cytokine of interest—IFN- γ .

Several observations can be made by comparing the response of NW and planar aptasensors. First, signal suppression values are almost $2\times$ higher for nanostructured surfaces compared to planar electrodes. Signal suppression is a normalized change in redox signal and describes aptamer–analyte engagement events that lead to a change in redox current. This normalization process eliminates electrode surface area of NW electrodes as a factor contributing to signal enhancement. It would appear that NW aptasensors are either more efficient at binding cytokine molecules compared to planar aptasensors or are better at relaying change in electrochemical signal due to cytokine binding events. The first explanation is supported by an observation that aptamer surface density on NW electrodes is >2 -fold higher compared to planar electrodes.

Interactions of Cells with NW Substrates. In the next set of experiments we wanted to characterize the nature of T-cell interactions with nanostructured surfaces. T-cells suspended in RPMI at 500,000 cell/mL were incubated with planar and NW surfaces for 2 h. This is an approximate time frame of a cytokine detection experiment. Subsequently, surfaces were imaged by SEM Figure 3a,b demonstrates T-cells on substrates containing 6- μm -long, 100-nm-diameter NWs spaced out by 2 to 10 μm . As seen from these images, cells were captured between

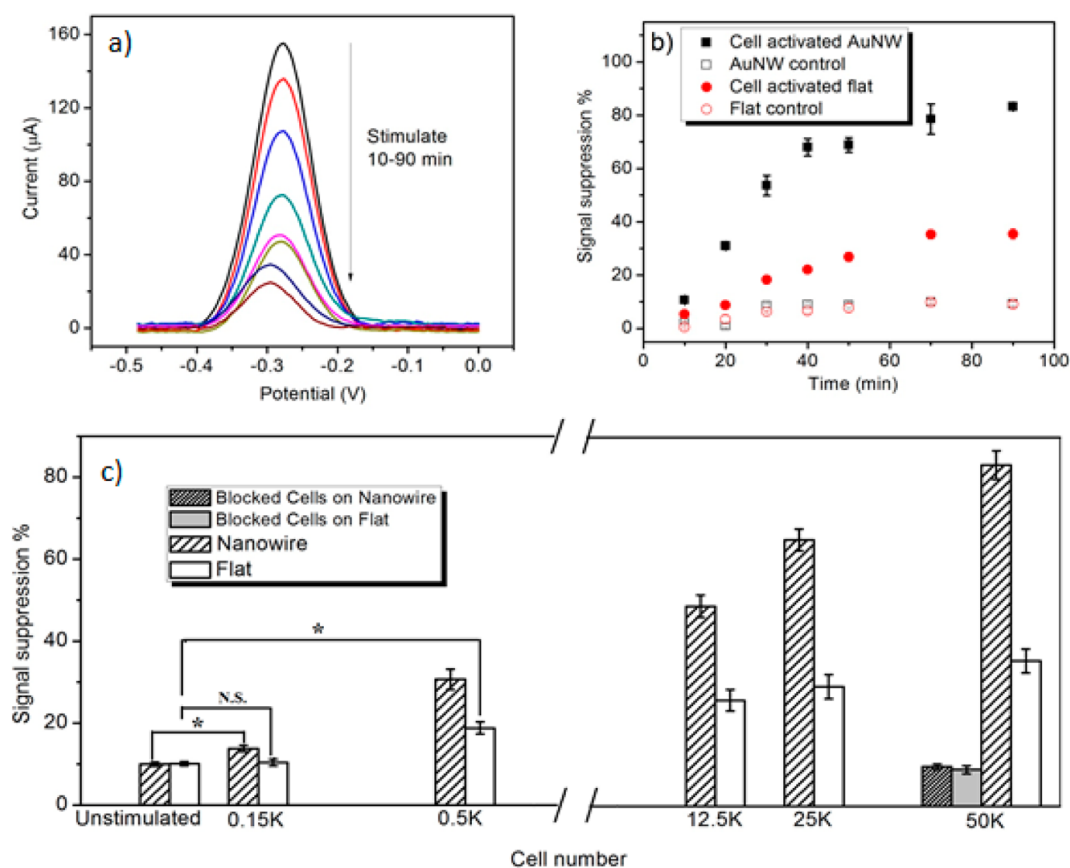


Figure 4. Detecting IFN- γ release from leukocytes with NW aptasensors. (a) Continuous monitoring of IFN- γ release from cells using AuNWs aptasensor. Cytokine are produced from activated PBMC cells, measurements were made for 90 min and the redox peak decreased in response to cytokine secretion. (b) Changes in redox peak were converted into signal suppression and plotted against measurement time for 50K stimulated PBMC cell (black solid square) and 50K unstimulated PBMC cell control (black open square) on AuNW electrode, and 50K stimulated PBMC cell (red solid circle) and 50K unstimulated PBMC cell control (red open circle). (c) Comparison of AuNWs aptasensor (dense packing) and flat aptasensor (blank) responses to different number of cells secreted. The cells were activated for 100 min for all different cell numbers and the signal suppressions were calculated by measuring redox peak decrease. The data indicates means \pm SD ($n = 3$). * $P < 0.05$.

individual nanowires but not impaled on the nanowires. Based on these observations it was possible to presume that NW electrodes will be available for detection of extracellular, secreted molecules such as IFN- γ . In the case of high cell concentration, deposition of cells onto a planar electrode surface may result in obstruction of recognition sites and loss of the sensor function. As highlighted by images in Figure 3a,b, such obstruction may not affect aptamer-functionalized NWs which remain free of cells and available for detection of cell-secreted molecules. Importantly, interactions with NW surfaces did not compromise viability of cells. Live/dead staining (not shown here) revealed that 88% of cells were viable when incubated with planar and NW electrodes under physiological conditions for 4 h.

Effect of Geometry on NW Aptasensor Performance.

In the next set of experiments we sought to characterize how aptasensors with NWs of varying geometries responded to IFN- γ . 50,000 T-cells were placed into a 0.5 mL solution of an E-cell. The cells were mitogenically stimulated to secrete cytokines and were maintained at physiological conditions (37 °C, 5% CO₂) for 2 h. SWV analysis was undertaken to characterize aptasensor responses to T-cell-secreted IFN- γ . The geometries tested included 6- μ m-long NWs with 30, 100, and 200 nm diameters. As described in the Experimental Section, different density of Au NPs in the respective colloidal solutions

resulted in an average inter-NW spacing between ≈ 300 nm for 30 nm NWs and ≈ 10 μ m for larger diameter NWs. Figure 3c highlights geometry dependent responses of aptasensors with 100-nm-diameter wires providing highest change in the redox current (80% signal suppression) while 30 nm wires recorded only a 20% change in redox signal. Therefore, our results demonstrate that the geometry and density of 100 nm wires is most suitable for cell detection experiments. It is likely that the spatial arrangement of this nanostructure substrate allowed for cells to land between the wires without impeding electron transfer.

We also characterized effects of NW length on sensor responses. In this case, NW diameter was fixed at 100 nm and length was varied from 6 to 60 μ m to 160 μ m. The differences in NW aptasensor responses to secreted IFN- γ were not as dramatic as those seen for varying NW diameters (Figure 3b). These differences may be attributed to decrease in physical robustness of NWs as a function of NW length. We found that a significant fraction of longer NWs was lying flat on the surface; hence, they were likely not fully capable of capturing secreted cytokine molecules.

Detection of IFN- γ Release from Immune Cells. In the next set of experiments, we proceeded to characterize responses of nanowire aptasensors to cell-secreted IFN- γ . These experiments were carried out with NWs of 100 nm in diameter and 6

μm in length. CD4 T-cells were first isolated from human blood, and then resuspended in RPMI at the desired concentration and dispensed into e-cells containing either planar or nanowire aptasensors. Once cells were inside an e-cell, mitogen (PMA/ionomycin) was added to trigger cytokine release from cells. Figure 4a,b summarizes cytokine secretion experiment with 50,000 cells residing in an e-cell (volume of 0.5 mL). SWV measurements were made every 10 min for the first 50 min and every 20 min after that. As seen from Figure 4b, NW aptasensors responded rapidly reaching 69% signal suppression in the first 50 min of stimulation and saturating at 83% after 90 min. The response of NW aptasensors was considerably faster than that of planar aptasensors. In the first 30 min of interaction with activated immune cells, response of nanowire aptasensor reached 70% of the maximum whereas planar aptasensor was at $\sim 55\%$. Because the change of redox signal due to analyte binding was a lot greater for nanowire aptasensors, it was possible to achieve 9- to 10-fold increase in signal after 30 min of interaction with cytokine producing cells. In comparison, signal suppression for planar aptasensors ranged from 5% in the absence of IFN- γ to 35% at saturation—thus only a 6-fold increase over the background was possible to this aptasensor. The fold difference over background at 30 min was ~ 3 .

An important question addressed in this study was related to the lowest number of cells that can be detected with planar vs nanowire aptasensors. This question is pertinent to clinical situations where CD4 T-cell counts are low and signal due to secreted IFN- γ is weak. One prominent clinical situation where such a scenario is encountered is in patients coinfecting with HIV and TB. Such coinfections are common in countries where both of these diseases are endemic (e.g., Sub-Saharan Africa). HIV/AIDS patients can have CD4 T-cell counts of 200 cell/ μL or less.^{32,33} Assuming that TB-specific memory T-cells in such patients constitute between 0.1% and 1% of the total CD4 T-cell population, there will only be between 200 and 2000 IFN- γ producing CD4 T-cells per mL of patient blood. Therefore, we tested responses of planar and NW aptasensors to T-cells varying in concentration from 300 to 50,000 cells per mL. Figure 4c shows that both planar and NW electrodes were sensitive in detecting IFN- γ release from very few T-cells. However, NW aptasensors showed responses to as few as 300 cells/mL, whereas planar aptasensors were not sensitive enough to detect secretions from such a low number of cells.

In light of improved sensitivity of NW aptasensors, we carried out additional control experiments to prove that electrochemical signals were indeed due to secreted IFN- γ . We have tested specificity of IFN- γ aptasensors extensively by challenges with nonsense proteins commonly present in serum (see Figure 3d and ref 30); however, there remained a possibility that these experiments do not account for some unknown cell-secreted nonspecific signal capable of eliciting response of the sensor. As an additional strategy for validating specificity, we utilized chimeric anti-CD45/anti-IFN- γ Ab molecules. These commercially available chimeric Abs attach to pan leukocyte CD45 antigen and then capture secreted IFN- γ molecules. In this control experiment, T-cells collected from the same venipuncture were split into two samples: one sample was pretreated with chimeric antibodies whereas the other sample was not. Both samples were stimulated with mitogens. As shown in Figure 4c, pretreatment of T-cells (bars describing signals from 50,000 cells) with chimeric antibodies resulted in

aptasensor responses comparable to those for unactivated T-cells.

In another control experiment, we used ELISA measurements to verify that chimeric Abs interfered with IFN- γ but not another secreted cytokine, for example, TNF- α . Here, T-cells were preincubated with anti-IFN- γ chimeric Abs then mitogenically stimulated as described above. Subsequently, media was collected and analyzed for both IFN- γ and TNF- α . As shown in Figure 5a, chimeric Abs diminished the concentration of IFN- γ

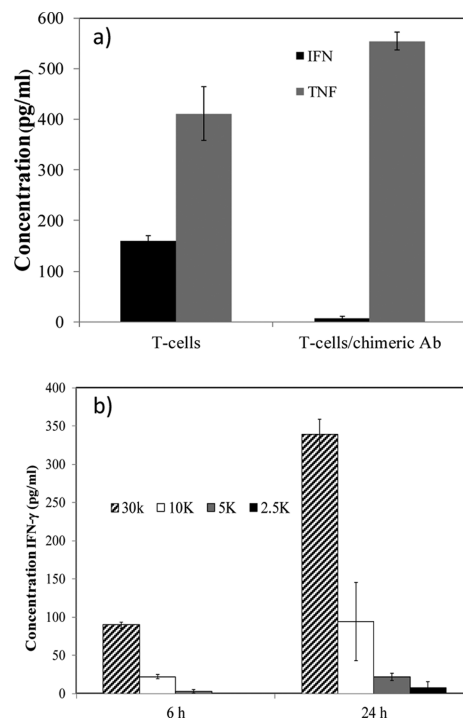


Figure 5. ELISA analysis of cytokine release from T-cells. (a) Release of IFN- γ and TNF- α from 30,000 T-cells after mitogenic stimulation. Incubation with chimeric anti-IFN- γ Abs decreased IFN- γ signal detected by ELISA while TNF- α levels remained largely unaffected. This data demonstrated that chimeric Abs bound to IFN- γ and did not affect other secreted cytokines such as TNF- α . (b) Varying concentrations of CD4 T-cells were stimulated in a 12-well plate and then analyzed by ELISA for IFN- γ production. Data represent $n = 3$ samples.

available for ELISA measurements while the level of TNF- α was largely unaffected. These results once again highlight that aptasensors responded to IFN- γ with high specificity.

To compare aptasensor performance to a standard method of IFN- γ detection, we carried out ELISA with T-cells of varying concentrations placed into a 24 well plate and stimulated with mitogen. After stimulation, cells were removed by centrifugation and remaining media was used to quantify secreted IFN- γ . The results in Figure 5b show that after 6 h mitogenic stimulation IFN- γ concentration ranged from 3 pg/mL for 5000 cells to 90 pg/mL for 30,000 cells. Significantly, secretion from 2500 cells was undetectable at 6 h time point but did become detectable after 24 h stimulation.

Why is our aptasensor more sensitive than ELISA? How do we reconcile the fact that the limit of detection for aptasensors ranges between 0.2 ng/mL and 1 ng/mL, whereas according to ELISA results in Figure 5, INF- γ is present in low pg/mL concentration? To better understand our scenario, please consider Scheme 1. In our detection approach, immune cells

reside in close proximity to the sensing surfaces such that high local concentration of secreted IFN- γ is detected at the electrode surface. In contrast, in an ELISA experiment, cells secrete into a large of volume of media which is then collected and placed into an ELISA plate to generate a read-out. Along the way, concentration gradients are disturbed, homogenized, and averaged out. We estimate that our method records 10- to 100-fold higher concentration than ELISA because of co-location of cells right next to the sensors.

CONCLUSION

This study demonstrates utility of NW aptasensors for detection of cell-secreted cytokines. We demonstrate that Au-coated NWs result in biosensors that have lower limit of detection and much better signal-to-noise ratio compared to planar Au aptasensors. NW aptasensors possess larger surface area per footprint, have higher aptamer packing density, and are minimally affected by direct deposition of leukocytes. Importantly, we highlight the fact these nanostructured aptasensors were more sensitive than planar aptasensors, capable of detection IFN- γ release from as few as 300 T-cells in mL of solution. IFN- γ release assays are used commonly for TB diagnosis. The ability to detect IFN- γ production in a blood sample containing few CD4 T-cells is critically important for TB patients with compromised immunity, for example, those coinfecting with HIV. Therefore, NW aptasensors described here may be used in the future to address an important need for more sensitive diagnosis of HIV/TB coinfections.

AUTHOR INFORMATION

Corresponding Author

*E-mail: revzin.alexander@mayo.edu.

ORCID

Ying Liu: 0000-0001-5718-7804

Alexander Revzin: 0000-0002-8737-3250

Author Contributions

[#]Ying Liu and Ali Rahimian contributed equally to this work. All authors have given approval to the final version of the manuscript.

Notes

The authors declare no competing financial interest.

ACKNOWLEDGMENTS

This study was funded in part by the National Science Foundation (CHE-1403561). Additional funding was provided by the Ministry of Education and Science of the Republic of Kazakhstan (grant no. 4132/GF4). Y.L. acknowledges support from the National Natural Science Foundation of China (grant no. 21605083) and the Natural Science Foundation of Jiangsu Province (BK20160644).

REFERENCES

- (1) Gao, Z. Q.; Agarwal, A.; Trigg, A. D.; Singh, N.; Fang, C.; Tung, C. H.; Fan, Y.; Buddharaju, K. D.; Kong, J. M. Silicon nanowire arrays for label-free detection of DNA. *Anal. Chem.* **2007**, *79* (9), 3291–3297.
- (2) Shao, M. W.; Shan, Y. Y.; Wong, N. B.; Lee, S. T. Silicon nanowire sensors for bioanalytical applications: Glucose and hydrogen peroxide detection. *Adv. Funct. Mater.* **2005**, *15* (9), 1478–1482.
- (3) Qi, S.; Yi, C.; Ji, S.; Fong, C.-C.; Yang, M. Cell Adhesion and Spreading Behavior on Vertically Aligned Silicon Nanowire Arrays. *ACS Appl. Mater. Interfaces* **2009**, *1* (1), 30–34.
- (4) Yoon, H. J.; Kozminsky, M.; Nagraath, S. Emerging Role of Nanomaterials in Circulating Tumor Cell Isolation and Analysis. *ACS Nano* **2014**, *8* (3), 1995–2017.
- (5) Kwon, N. H.; Beaux, M. F., II; Ebert, C.; Wang, L.; Lassiter, B. E.; Park, Y. H.; McIlroy, D. N.; Hovde, C. J.; Bohach, G. A. Nanowire-based delivery of Escherichia coli O157 Shiga toxin 1 A subunit into human and bovine cells. *Nano Lett.* **2007**, *7* (9), 2718–2723.
- (6) Tian, B.; Lieber, C. M. Synthetic Nanoelectronic Probes for Biological Cells and Tissues. *Annu. Rev. Anal. Chem.* **2013**, *6* (6), 31–51.
- (7) Shalek, A. K.; Robinson, J. T.; Karp, E. S.; Lee, J. S.; Ahn, D.-R.; Yoon, M.-H.; Sutton, A.; Jorgolli, M.; Gertner, R. S.; Gujral, T. S.; MacBeath, G.; Yang, E. G.; Park, H. Vertical silicon nanowires as a universal platform for delivering biomolecules into living cells. *Proc. Natl. Acad. Sci. U. S. A.* **2010**, *107* (5), 1870–1875.
- (8) Shalek, A. K.; Gaublomme, J. T.; Wang, L.; Yosef, N.; Chevrier, N.; Andersen, M. S.; Robinson, J. T.; Pochet, N.; Neuberger, D.; Gertner, R. S.; Amit, I.; Brown, J. R.; Hacohen, N.; Regev, A.; Wu, C. J.; Park, H. Nanowire-Mediated Delivery Enables Functional Interrogation of Primary Immune Cells: Application to the Analysis of Chronic Lymphocytic Leukemia. *Nano Lett.* **2012**, *12* (12), 6498–6504.
- (9) VanDersarl, J. J.; Xu, A. M.; Melosh, N. A. Nanostraws for Direct Fluidic Intracellular Access. *Nano Lett.* **2012**, *12* (8), 3881–3886.
- (10) Timko, B. P.; Cohen-Karni, T.; Qing, Q.; Tian, B.; Lieber, C. M. Design and Implementation of Functional Nanoelectronic Interfaces With Biomolecules, Cells, and Tissue Using Nanowire Device Arrays. *IEEE Trans. Nanotechnol.* **2010**, *9* (3), 269–280.
- (11) Duan, X.; Gao, R.; Xie, P.; Cohen-Karni, T.; Qing, Q.; Choe, H. S.; Tian, B.; Jiang, X.; Lieber, C. M. Intracellular recordings of action potentials by an extracellular nanoscale field-effect transistor. *Nat. Nanotechnol.* **2011**, *7* (3), 174–179.
- (12) Gao, R.; Strehle, S.; Tian, B.; Cohen-Karni, T.; Xie, P.; Duan, X.; Qing, Q.; Lieber, C. M. Outside Looking In: Nanotube Transistor Intracellular Sensors. *Nano Lett.* **2012**, *12* (6), 3329–3333.
- (13) Lapierre, M. A.; O’Keefe, M.; Taft, B. J.; Kelley, S. O. Electrochemical detection of pathogenic DNA sequences and antibiotic resistance markers. *Anal. Chem.* **2003**, *75* (22), 6327–6333.
- (14) Das, J.; Kelley, S. O. Tuning the Bacterial Detection Sensitivity of Nanostructured Microelectrodes. *Anal. Chem.* **2013**, *85* (15), 7333–7338.
- (15) Vasilyeva, E.; Lam, B.; Fang, Z.; Minden, M. D.; Sargent, E. H.; Kelley, S. O. Direct Genetic Analysis of Ten Cancer Cells: Tuning Sensor Structure and Molecular Probe Design for Efficient mRNA Capture. *Angew. Chem., Int. Ed.* **2011**, *50* (18), 4137–4141.
- (16) Matharu, Z.; Enomoto, J.; Revzin, A. Miniature Enzyme-Based Electrodes for Detection of Hydrogen Peroxide Release from Alcohol-Injured Hepatocytes. *Anal. Chem.* **2013**, *85* (2), 932–939.
- (17) Son, K. J.; Shin, D.-S.; Kwa, T.; Gao, Y.; Revzin, A. Micropatterned Sensing Hydrogels Integrated with Reconfigurable Microfluidics for Detecting Protease Release from Cells. *Anal. Chem.* **2013**, *85* (24), 11893–11901.
- (18) Matharu, Z.; Patel, D.; Gao, Y.; Hague, A.; Zhou, Q.; Revzin, A. Detecting Transforming Growth Factor-beta Release from Liver Cells Using an Aptasensor Integrated with Microfluidics. *Anal. Chem.* **2014**, *86* (17), 8865–8872.
- (19) Liu, Y.; Yan, J.; Howland, M. C.; Kwa, T.; Revzin, A. Micropatterned Aptasensors for Continuous Monitoring of Cytokine Release from Human Leukocytes. *Anal. Chem.* **2011**, *83* (21), 8286–8292.
- (20) Liu, Y.; Zhou, Q.; Revzin, A. An aptasensor for electrochemical detection of tumor necrosis factor in human blood. *Analyst* **2013**, *138* (15), 4321–4326.
- (21) Kwa, T.; Zhou, Q.; Gao, Y.; Rahimian, A.; Kwon, L.; Liu, Y.; Revzin, A. Reconfigurable microfluidics with integrated aptasensors for monitoring intercellular communication. *Lab Chip* **2014**, *14* (10), 1695–1704.

- (22) Ying, L.; Matharu, Z.; Rahimian, A.; Revzin, A. Detecting multiple cell-secreted cytokines from the same aptamer-functionalized electrode. *Biosens. Bioelectron.* **2015**, *64*, 43–50.
- (23) Liu, Y.; Kwa, T.; Revzin, A. Simultaneous detection of cell-secreted TNF-alpha, and IFN-gamma using micropatterned aptamer-modified electrodes. *Biomaterials* **2012**, *33* (30), 7347–7355.
- (24) Xiao, Y.; Lai, R. Y.; Plaxco, K. W. Preparation of electrode-immobilized, redox-modified oligonucleotides for electrochemical DNA and aptamer-based sensing. *Nat. Protoc.* **2007**, *2* (11), 2875–2880.
- (25) Ferguson, B. S.; Hoggarth, D. A.; Maliniak, D.; Ploense, K.; White, R. J.; Woodward, N.; Hsieh, K.; Bonham, A. J.; Eisenstein, M.; Kippin, T. E.; Plaxco, K. W.; Soh, H. T. Real-Time, Aptamer-Based Tracking of Circulating Therapeutic Agents in Living Animals. *Sci. Transl. Med.* **2013**, *5* (213), 213ra165.
- (26) Wu, C.; Wan, S.; Hou, W.; Zhang, L.; Xu, J.; Cui, C.; Wang, Y.; Hu, J.; Tan, W. A survey of advancements in nucleic acid-based logic gates and computing for applications in biotechnology and biomedicine. *Chem. Commun.* **2015**, *51* (18), 3723–3734.
- (27) Krylyuk, S.; Davydov, A. V.; Levin, I. Tapering Control of Si Nanowires Grown from SiCl₄ at Reduced Pressure. *ACS Nano* **2011**, *5* (1), 656–664.
- (28) Ricci, F.; Lai, R. Y.; Heeger, A. J.; Plaxco, K. W.; Sumner, J. J. Effect of molecular crowding on the response of an electrochemical DNA sensor. *Langmuir* **2007**, *23* (12), 6827–6834.
- (29) White, R. J.; Phares, N.; Lubin, A. A.; Xiao, Y.; Plaxco, K. W. Optimization of electrochemical aptamer-based sensors via optimization of probe packing density and surface chemistry. *Langmuir* **2008**, *24* (18), 10513–10518.
- (30) Liu, Y.; Tuleouva, N.; Ramanculov, E.; Revzin, A. Aptamer-Based Electrochemical Biosensor for Interferon Gamma Detection. *Anal. Chem.* **2010**, *82* (19), 8131–8136.
- (31) Hill, H. D.; Millstone, J. E.; Banholzer, M. J.; Mirkin, C. A. The Role Radius of Curvature Plays in Thiolated Oligonucleotide Loading on Gold Nanoparticles. *ACS Nano* **2009**, *3* (2), 418–424.
- (32) Getahun, H.; Gunneberg, C.; Granich, R.; Nunn, P. HIV Infection-Associated Tuberculosis: The Epidemiology and the Response. *Clin. Infect. Dis.* **2010**, *50*, S201–S207.
- (33) Pawlowski, A.; Jansson, M.; Skold, M.; Rottenberg, M. E.; Kallenius, G. Tuberculosis and HIV Co-Infection. *PLoS Pathog.* **2012**, *8* (2), e1002464.

Supporting Information

Electrochemical Detection of Acetaminophen Using Silicon Nanowires

Raja Ram Pandey¹, Hussain S. Alshahrani,¹ Sergiy Krylyuk,^{2,3} Elissa H. Williams,³ Albert V. Davydov,³ and Charles C. Chusuei^{1,*}

¹Chemistry Department, 440 Friendship Street, Middle Tennessee State University, Murfreesboro, TN 37132, USA

²Theiss Research, La Jolla, CA 92037, USA

³Materials Science and Engineering Division, Material Measurement Laboratory, National Institute of Standards and Technology, Gaithersburg, MD 20899, USA

1. Surface Characterization by SEM, EDX, ATR-IR, and XPS

Scanning electron micrographs (SEMs) of the SiNWs were used to quantify the surface density of material deposited onto the electrodes for electrochemical analysis. SEM analysis was performed using a Hitachi S3400N SEM operated at 15 kV with 18,000x magnification. **Figure S1** shows a representative SEM image of the rod-shaped SiNWs.

Energy dispersive X-ray (EDX) spectroscopy of the SiNWs was used to analyze the elemental composition present in the composite. EDX analysis was performed using Oxford Inca X-act instrument. **Figure S2** shows the SEM image of the SiNWs accompanying the EDX data, indicating Si and O present on the GCE surface. EDX scans of the SiNWs deposited on the electrode surface had an average atomic percent composition of $66 \pm 8\%$ O and $34 \pm 8\%$ Si from $n = 6$ samplings.

ATR-IR analysis was carried out using a Varian 7000 FTIR with a mercury cadmium telluride (MCT) detector and Varian Resolution Pro software, ver. 5.0 (Randolph, MA, USA). The detector was cooled with liquid nitrogen (LN₂) and data was obtained after a 30 min equilibration time. Air was used for background subtraction. A Golden Gate ATR diamond crystal was used as the support in the instrument's sample compartment. ATR-IR spectra of SiNWs is shown in **Figure S3** along with that of isopropanol (background solvent). The two peaks with asterisk signs at 1546 and 1742 cm⁻¹ are attributed to the SiCH=CH₃ and SiO-C-OCH₃ vibrations [1], respectively. Other peaks are attributed to artifacts from isopropanol in which SiNWs were

dispersed. The spectrum of SiNWs was obtained after depositing and drying 600 μL of SiNWs solution on the crystal of the ATR-IR instrument.

XPS measurements were performed using a Perkin Elmer PHI 560 instrument with a 25-270AR double-pass cylindrical mirror analyzer operated at 12 kV and 225 W with a Mg K α anode using a photon energy of $h\nu = 1253.6$ eV. A binding energy (BE) of 284.7 eV for the C 1s orbital, denoting adventitious carbon [2], was used for charge referencing. Shirley background subtractions for Si 2p and O 1s peaks were used. Deconvolutions were performed using a 70 % to 30 % Gaussian-Lorentzian line-shape with the assistance of CasaXPS software, version 2.2.107 (Devon, United Kingdom). To perform the scans, a Si (100) wafer containing the SiNWs was mounted onto the XPS sample holder, and outgassed in a turbo-pumped antechamber. The system pressure did not exceed 1.0×10^{-8} Torr during XPS analysis. XPS high resolution narrow scans for O 1s, C 1s and Si 2p were carried out. Atomic percent composition measured from the C 1s, O 1s and Si 2p orbitals, after normalizing their integrated peak areas to their atomic sensitivity factors [3], were 19.4 %, 74.0 % and 6.5 %, respectively. **Figure S4 (A)** presents the O 1s XPS spectrum for SiNWs. XPS spectra of O 1s orbitals for the SiNWs was curvefitted using the same BE positions and line-shapes for SiNWs reported by Lamaa et al. [4] for reference positions (**Figure S4A**). BE peak centers (with full-width-at-half-maxima in parentheses) were fixed at 531.6 (2.0) and 532.7 (2.0) eV, denoting SiO₂ and adsorbed hydroxyls, respectively. **Figure S4 (B)** displays the XPS spectrum of silicon which provides two Si 2p peaks at 103.0 (2.3) eV and 99.1 (1.8) eV related to silicon oxide and silicon, respectively.

2. Optimum SiNW Loading Density

Figure S5 (A) shows CV responses determined using various SiNWs loadings. **Figure S5 (B)** demonstrates that both cathodic (reduction) and anodic (oxidation) currents are highest at a 20- μL loading corresponding to approximately $1.4 (\pm 0.5) \times 10^3$ SiNWs/ mm^2 based on an average of $n = 53$ SEM images. The SiNWs were applied to the GCE surface using droplets corresponding to an estimated 7×10^2 SiNWs per 10- μL droplet applied in each application. SiNW loadings above or below the 20- μL aliquot total volume resulted in reduced current observed for APAP detection.

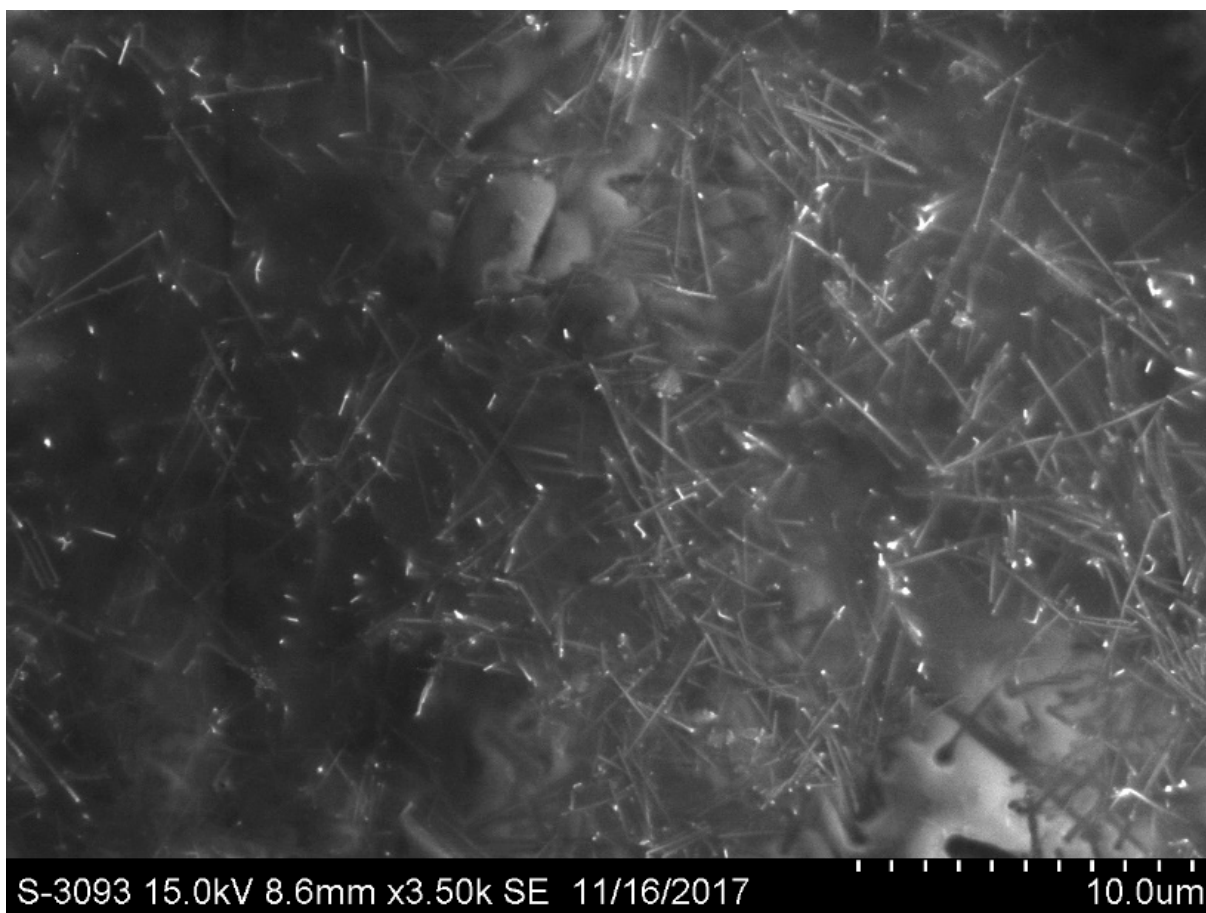


Figure S1. Representative SEM of 30 nm diam SiNWs deposited on the GCE after sonication.

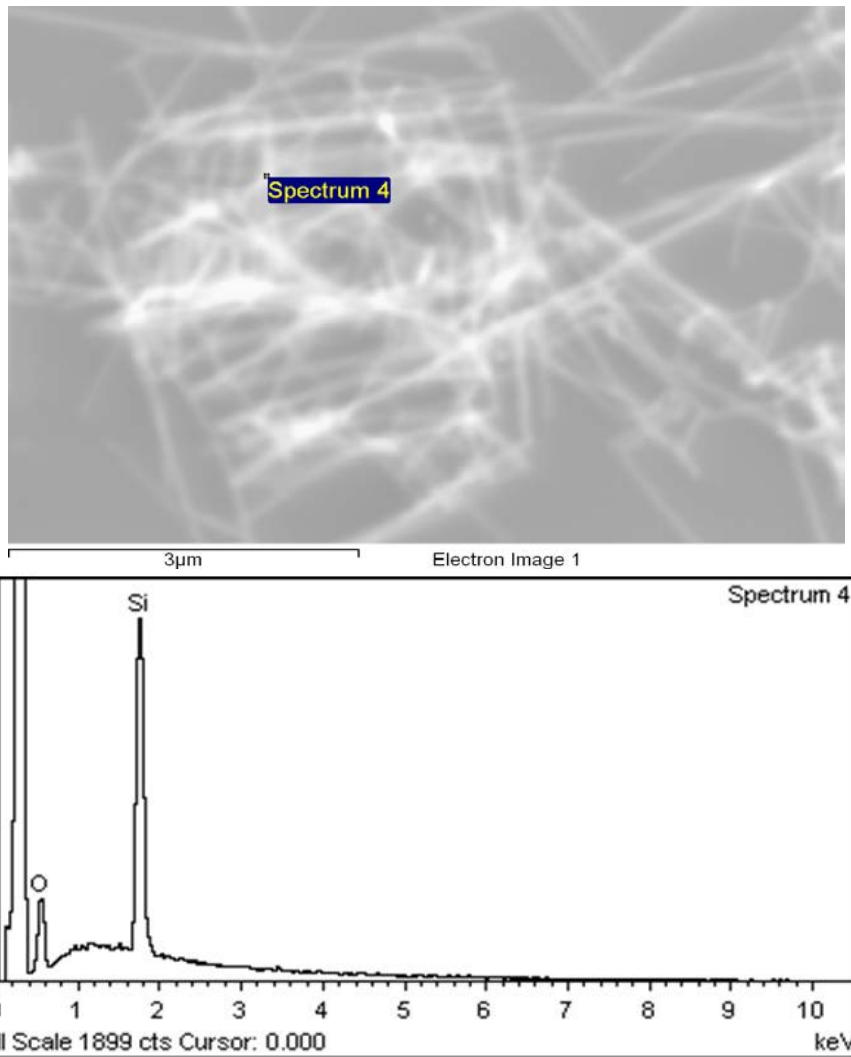


Figure S2. EDX image and spectrum of 30 nm diam SiNWs on GCE.

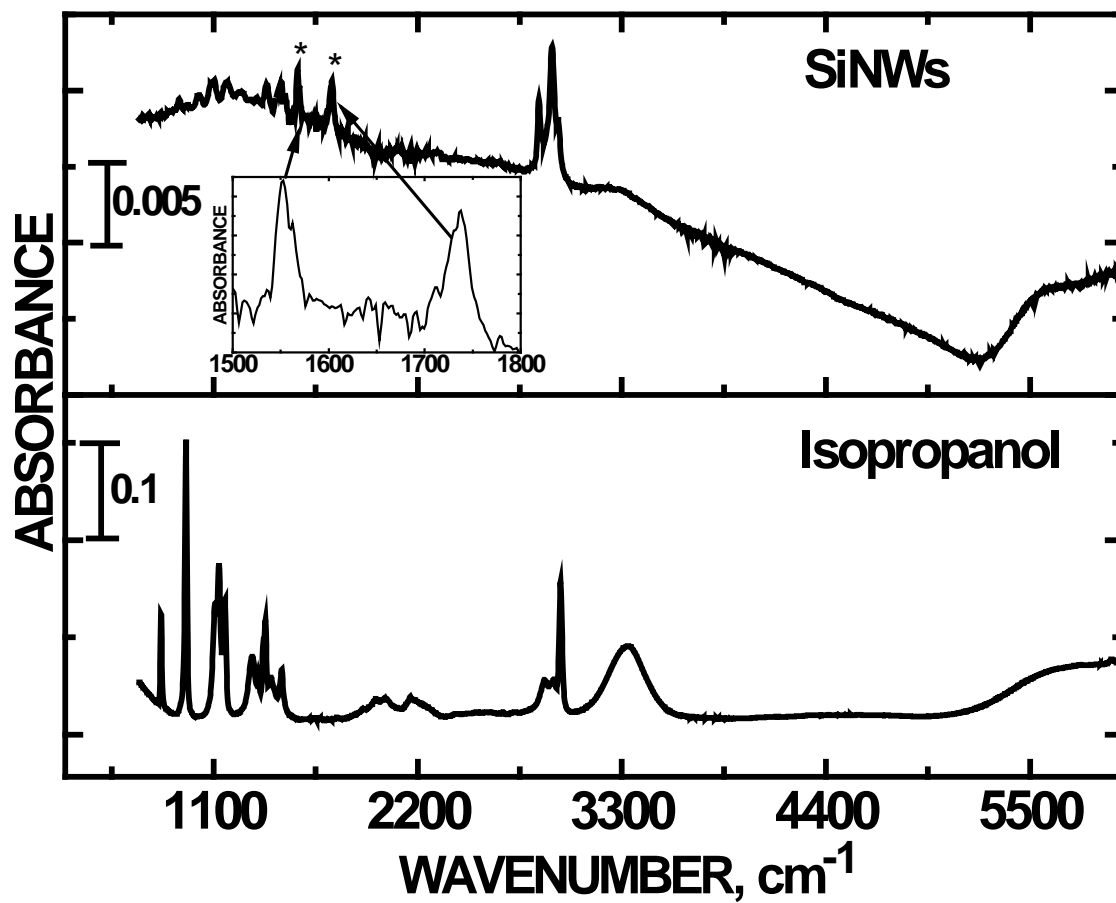


Figure S3. ATR-IR spectra of SiNWs (top) and isopropanol (bottom) along with inset showing the expanded form of the two peaks (in asterisks) attributed to SiNWs.

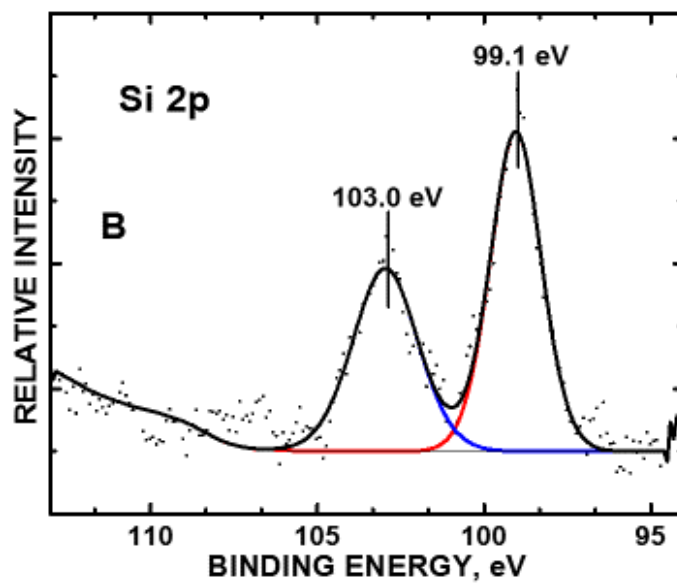
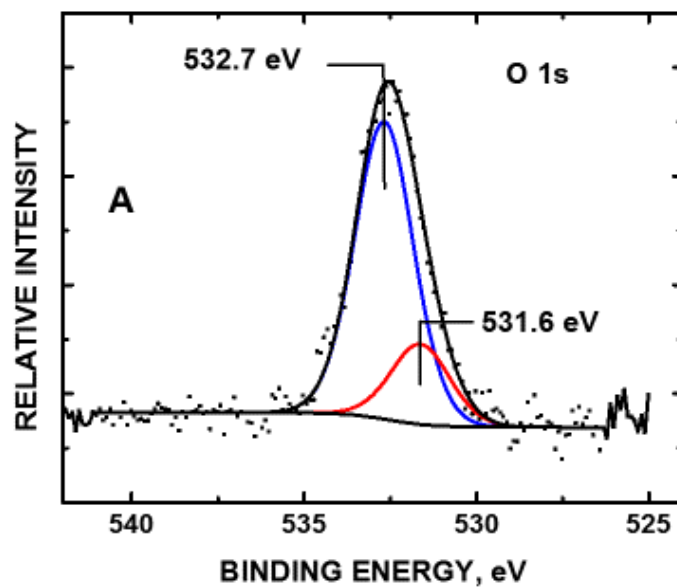


Figure S4. XPS narrow scans of the (A) O 1s, and (B) Si 2p core orbitals of SiNWs.

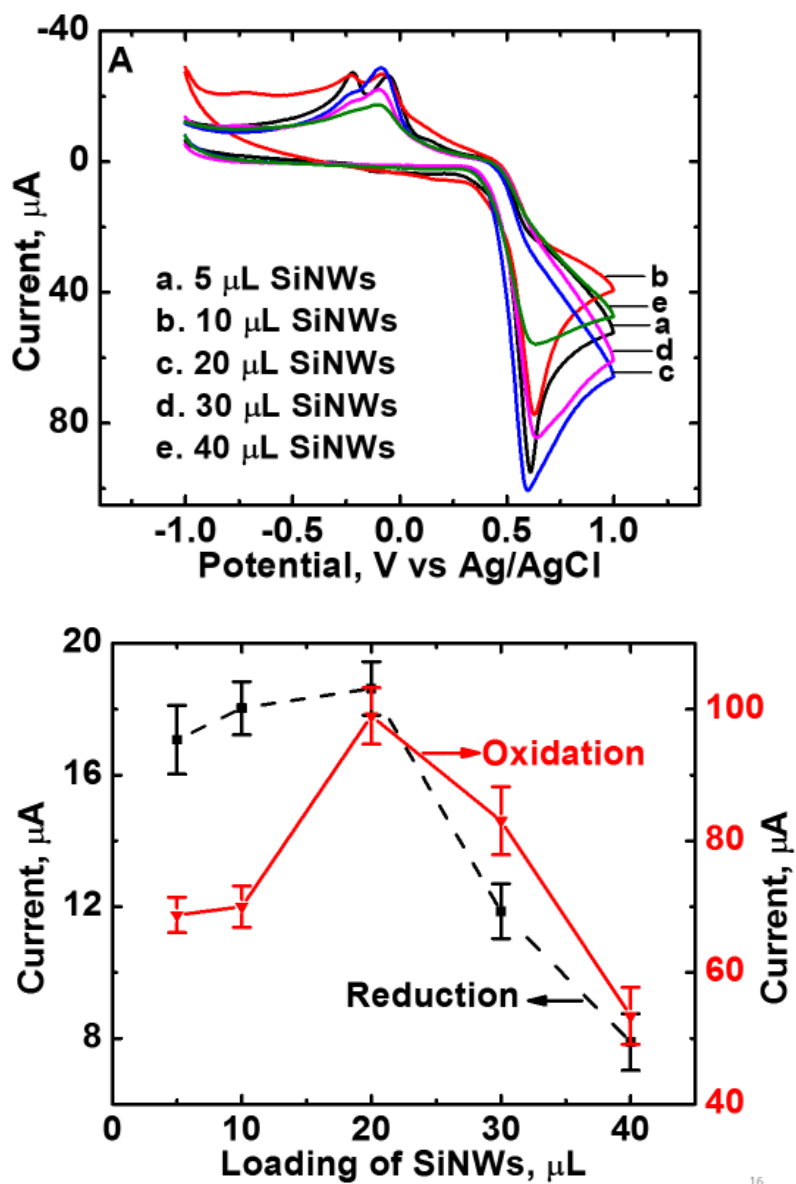


Figure S5. (A) CVs of Nafion/SiNW/GCE in 10 mmol dm⁻³ APAP at pH = 7.4 with different loadings of SiNWs at 50 mV s⁻¹ scan rate. (B) Reduction and oxidation peak current vs SiNW loading.

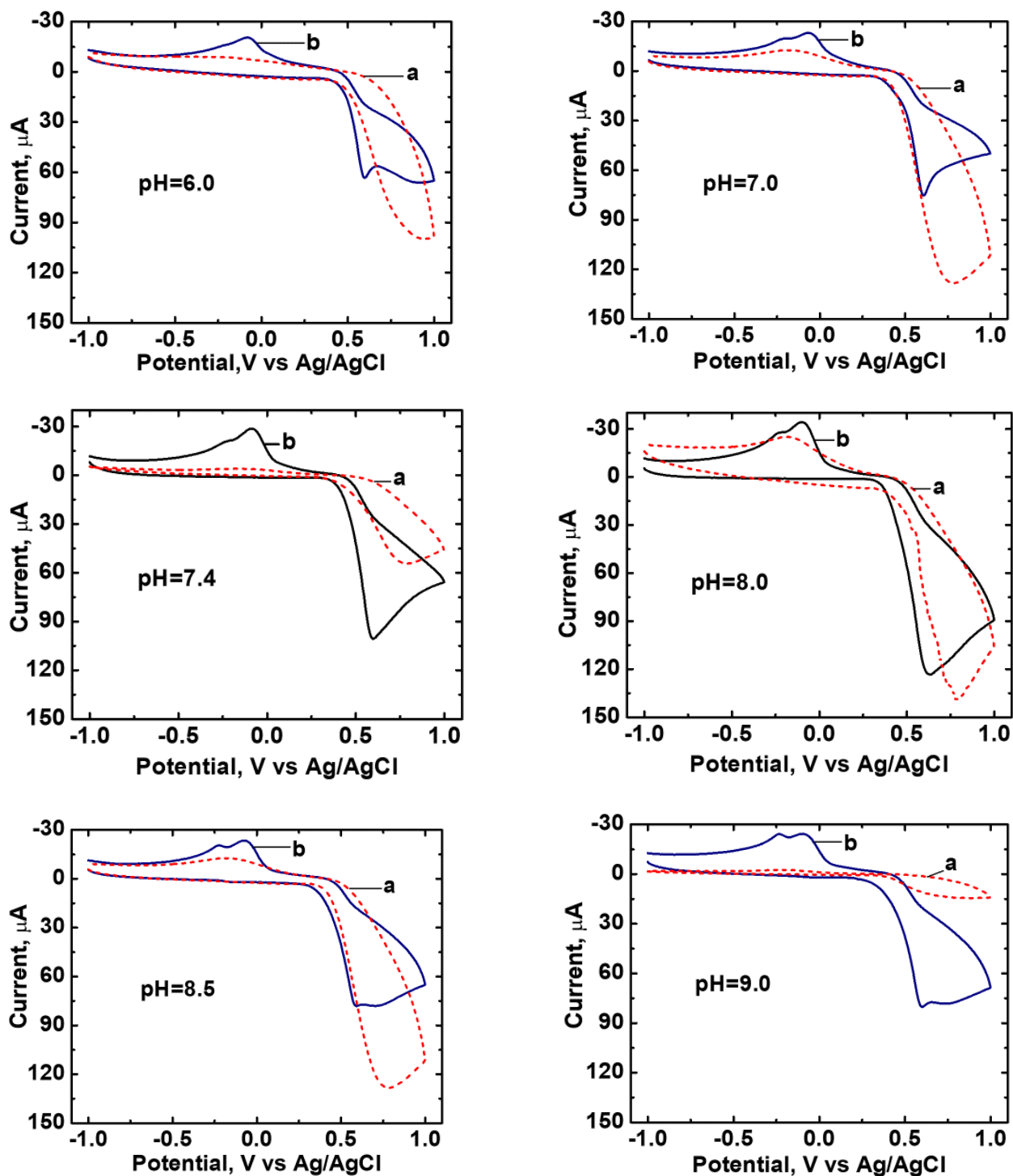


Figure S6. CVs of (a) bare GCE and (b) Nafion/SiNWs/GCE in 10 mmol dm^{-3} APAP in N_2 -saturated phosphate buffer with pH = 6.0 to 9.0 at a scan rate of 50 mV s^{-1} .

References

- [1] A. L. Smith, *Applied Infrared Spectroscopy*, Wiley and Sons: New York, 1979.
- [2] T. L. Barr, S. Seal, Nature of the use of adventitious carbon as a binding energy standard. *J. Vac. Sci. Technol. A* **1995**, 13, 1239-1246.
- [3] C. D. Wagner, L. E. Davis, M. V. Zeller, J. A. Taylor, R. H. Raymond, L. H. Gale, Empirical atomic sensitivity factors for quantitative analysis by electron spectroscopy for chemical analysis. *Surf. Interface Anal.* **1981**, 3, 211-225.
- [4] L. Lamaa, C. Ferronato, S. Prakash, L. Fine, F. Jaber, J. M. Chovelon, Photocatalytic oxidation of octamethyl cyclotetrasiloxane (D₄): Towards a better understanding of the impact of volatile methyl siloxanes on photocatalytic systems. *Appl. Catal. B: Environ* **2014**, 156, 438-446.

Table S1. Calculation of Diffusion Coefficients

| | | |
|----------|---|--|
| F | 96485.3329 C | $I_p = 0.4961 \text{ nFA } C_o^* \left(\frac{\alpha n F v D_E}{RT} \right)^{1/2}$ |
| R | 8.314 J mol ⁻¹ K ⁻¹ | |
| T | 295.15 K | Using this equation, αD was calculated as |
| n | 2 | |
| A | 0.19625 cm ² | $\alpha D_E = \frac{(I_p)^2 RT}{nF(\sqrt{v})^2 (0.4961 nFA C_o^*)^2}$ |
| C_o^* | 0.00001 moles cm ⁻³ | |
| constant | 0.4961 | |

For oxidation:

| $v^{1/2}$ (V) | i_{pa} (A) | αD (cm ² s ⁻¹) | |
|---------------|--------------|--|----------|
| 0.00316 | 3.199E-05 | 3.692E-05 | |
| 0.00447 | 3.586E-05 | 2.319E-05 | |
| 0.00547 | 3.967E-05 | 1.895E-05 | |
| 0.00632 | 4.284E-05 | 1.656E-05 | |
| 0.00707 | 4.650E-05 | 1.558E-05 | |
| 0.00774 | 4.989E-05 | 1.497E-05 | |
| 0.00836 | 5.258E-05 | 1.425E-05 | |
| 0.00894 | 5.517E-05 | 1.372E-05 | |
| 0.00948 | 5.774E-05 | 1.336E-05 | |
| 0.01000 | 5.975E-05 | 1.286E-05 | |
| 0.01048 | 6.401E-05 | 1.344E-05 | STD |
| | average = | 1.762E-05 | 7.09E-06 |

For reduction :

| $v^{1/2}$ (V) | i_{pa} (A) | αD (cm ² s ⁻¹) | |
|---------------|--------------|--|----------|
| 0.00316 | 5.000E-06 | 9.019E-07 | |
| 0.00447 | 8.002E-06 | 1.155E-06 | |
| 0.00547 | 9.502E-06 | 1.087E-06 | |
| 0.00632 | 9.991E-06 | 9.002E-07 | |
| 0.00707 | 1.049E-05 | 7.931E-07 | |
| 0.00774 | 1.199E-05 | 8.650E-07 | |
| 0.00836 | 1.262E-05 | 8.212E-07 | |
| 0.00894 | 1.348E-05 | 8.189E-07 | |
| 0.00948 | 1.419E-05 | 8.073E-07 | |
| 0.01000 | 1.514E-05 | 8.260E-07 | |
| 0.01048 | 1.639E-05 | 8.812E-07 | STD |
| | average = | 8.960E-07 | 1.18E-07 |